JHEP

Published for SISSA by Springer

Received: August 27, 2020
Revised: November 30, 2020
Accepted: February 22, 2021
Published: April 2, 2021

Atomki anomaly in gauged $\mathrm{U}(1)_R$ symmetric model

Osamu Seto[a,b] **and Takashi Shimomura**[c]

[a] *Institute for the Advancement of Higher Education, Hokkaido University, Sapporo 060-0817, Japan*
[b] *Department of Physics, Hokkaido University, Sapporo 060-0810, Japan*
[c] *Faculty of Education, Miyazaki University, Miyazaki, 889-2192, Japan*

E-mail: seto@particle.sci.hokudai.ac.jp, shimomura@cc.miyazaki-u.ac.jp

Abstract: The Atomki collaboration has reported that unexpected excesses have been observed in the rare decays of Beryllium nucleus. It is claimed that such excesses can suggest the existence of a new boson, called X, with the mass of about 17 MeV. To solve the Atomki anomaly, we consider a model with gauged $\mathrm{U}(1)_R$ symmetry and identify the new gauge boson with the X boson. We also introduce two SU(2) doublet Higgs bosons and one singlet Higgs boson, and discuss a very stringent constraint from neutrino-electron scattering. It is found that the $\mathrm{U}(1)_R$ charges of the doublet scalars are determined to evade the constraint. In the end, we find the parameter region in which the Atomki signal and all experimental constraints can be simultaneously satisfied.

Keywords: Beyond Standard Model, Gauge Symmetry

ArXiv ePrint: 2006.05497

https://doi.org/10.1007/JHEP04(2021)025

JHEP04(2021)025

Contents

JHEP04(2021)025

1 Introduction

The Atomki collaboration has been reporting results that unexpected excesses were found in the Internal Pair Creation (IPC) decay of Beryllium (Be) [1–5] and Helium (He) [6, 7] nuclei. In the reports, the excesses appear as bumps in the distributions of the invariant mass and opening angle of an emitted positron (e^+) and electron (e^-) pair from the IPC decays of ^{8}Be* and ^{4}He,

$$^8\text{Be}^*(18.15\text{ MeV}) \to {}^8\text{Be} + e^+ + e^-, \tag{1.1}$$

$$^4\text{He}(21.01\text{ MeV}) \to {}^4\text{He} + e^+ + e^-, \tag{1.2}$$

respectively. These bumps seem not to be explained within the standard nuclear physics [8], even if parity violating decays are taken into account. The collaboration reported that the

bumps can be well fitted simultaneously under the assumption that a hypothetical boson X with the mass of 17.01 ± 0.16 and $19.68 \pm 0.25\,\mathrm{MeV}$ is produced through $^8\mathrm{Be}^*$ and $^4\mathrm{He}$ decays, followed by X decay into a e^+-e^- pair, respectively. Such a light boson does not exist in the Standard Model (SM) of particle physics. Therefore, the anomaly can be considered as a signal of new physics beyond the SM.

The hypothetical boson X, in principle, can be a vector, axial-vector, scalar and pseudo-scalar boson. Among these possibilities, the scalar boson hypothesis is discarded due to the conservation of angular momentum in the decay eq. (1.1) [9, 10]. The vector boson hypothesis was firstly studied in [9, 10] in a gauged $B - L$ symmetric model, taking various experimental constraints into account. Then, many models have been proposed in contexts of an extra U(1) gauge symmetry [11–13], dark matter [14–16], neutrino physics [17], lepton anomalous magnetic moments [18–20] and others [21–25]. Experimental searches of the X boson are also studied in [26–29]. In [10], it was shown that there are two restrictive constraints to explain the Atomki anomaly. The first constraint comes from the rare decay of neutral pion, $\pi^0 \to \gamma X$, measured by the NA48/2 experiment. This constraint sets a very stringent bound on the coupling of X to proton because the decay branching ratio of the rare decay is scaled by the proton coupling. From this fact, such a vector boson is named as a protophobic boson. The second constraint comes from neutrino-electron scattering measured by the TEXONO experiment. It is difficult to evade this constraint and neutral pion constraint simultaneously. Therefore, new leptonic states are introduced to evade this constraint in [10], or no interaction of the X boson to active neutrinos is ad hoc assumed.

An axial-vector boson hypothesis also has been studied in [30]. This hypothesis has two advantages. One is that the constraints from the neutral pion decay can be easily evaded because the decay receives no contribution from the axial anomaly. The other advantage is that the partial decay width of $^8\mathrm{Be}^*$ is proportional to k_X,[1] the X's three momentum, while it is proportional to k_X^3 in the vector boson hypothesis. Because of this momentum dependence, coupling constants of X to quarks can be much smaller to explain the Atomki anomaly than that in the vector-boson hypothesis case. Then, it is possible to evade several experimental constraints in the axial-vector boson hypothesis. Several models with axial-vector boson have been proposed in [31–33]. In spite of these advantages, the constraint from neutrino-electron scattering is still very stringent and requires to suppress neutrino couplings to X. In [30], it is assumed that the neutrino couplings to the X boson vanish, and in [31–33], the neutrino coupling is assumed to be enough small. In the end, the pseudo-scalar hypothesis was studied in [34]. Decay widths of these three hypotheses are found in [35].

In this work, we pursue the axial-vector hypothesis and consider a $\mathrm{U}(1)_R$ gauge symmetry [36] where the gauge boson is identified with the X boson. The $\mathrm{U}(1)_R$ gauge symmetry is defined that only right-handed fermions are charged while left-handed ones are not charged. Then, the $\mathrm{U}(1)_R$ gauge boson has both vectorial and axial interactions to

[1]There is also k_X^3 term in the partial width. Following the discussion in [30], we neglected that term, which would be suppressed because k_X is smaller than the mass of the X boson.

JHEP04(2021)025

fermions. The existence of the axial interaction allows coupling constants to be smaller to satisfy the Atomki signal. With smaller couplings, a contribution to neutral pion decay from vectorial interactions is much suppressed. It was shown in [37, 38] that flavour changing neutral currents can be suppressed due to $U(1)_R$ symmetry in two Higgs doublet extension. It was also shown in [39–43] that neutrino masses and mixing, dark matter and the muon anomalous magnetic moment can be explained in models with the $U(1)_R$ gauge symmetry. Motivated by these previous works, we construct a minimal model to explain the Atomki anomaly with $U(1)_R$ gauge symmetry.

This paper is organized as follows. In section 2, we introduce our model as a minimal setup to explain the Atomki anomaly. In section 3, we give the coupling constants of fermions to the X boson and show the allowed region of the gauge coupling constants. Then, the signal requirement and experimental constraints are explained in section 4 and our numerical results are shown in section 5. In the end, we give our conclusion in section 6.

2 Model

We start our discussion by introducing our model. The gauge symmetry of the model is defined as $G_{\rm SM} \times U(1)_R$, where $G_{\rm SM}$ stands for the gauge symmetry of the SM. Under the $U(1)_R$ gauge symmetry, right-handed chiral fermions are charged while left-handed chiral ones are singlet [40]. Only with the SM matter content, such a charge assignment generally leads to non-vanishing gauge-anomalies due to $U(1)_R$ current contributions. Therefore, new fermions charged under $U(1)_R$ must be introduced to cancel the gauge anomalies. One of the simplest solutions for non-vanishing anomalies is to add three right-handed fermions, N_i $(i = 1, 2, 3)$, which are singlet under the SM gauge symmetries. The charge assignment of the fermions in our model is shown in table 1. In the table, $SU(3)$, $SU(2)_L$ and $U(1)_Y$ represent the SM strong, weak and hypercharge gauge groups. The symbols, Q and u_R, d_R represent left-handed quarks and right-handed up-type, down-type quarks, respectively, and L and e_R represent left-handed leptons and right-handed charged leptons, respectively. Without loss of generality, we can fix the $U(1)_R$ charge of u_R to $+\frac{1}{2}$ as the overall normalization. Then, the gauge charges of the other fermions are determined from anomaly-free conditions as shown in the table 1. For the Higgs field H_1, we assign its $U(1)_R$ charge to q_1, which can not be determined from anomaly-free conditions. However, if requiring the model to be minimal, q_1 should be taken as $+\frac{1}{2}$ so that quarks and charged leptons can form Yukawa interactions with H_1 in the same manner of the SM. Furthermore, with this charge assignment, left-handed neutrinos can form the Yukawa interaction with N_i. Therefore, we identify N_i as right-handed neutrinos in the following discussions.

To explain the Atomki anomaly, we further extend the matter content by adding a $SU(2)_L$ doublet scalar field H_2 and a $SU(2)_L$ singlet scalar field S. Firstly, it is shown in [44] that neutrinos can not be Dirac particles due to the constraints from $\Delta N_{\rm eff}$ unless the coupling constant of neutrinos are extremely small. This constraint can be avoided when right-handed neutrinos have Majorana masses. The $SU(2)_L$ singlet scalar field is introduced to give a mass to the X boson and Majorana masses to N_i after spontaneous breaking of $U(1)_R$. Thus its $U(1)_R$ charge is assigned to -1. The new $SU(2)_L$ doublet

JHEP04(2021)025

	Q	u_R	d_R	L	e_R	N	H_1	H_2	S
SU(3)	3	3	3	1	1	1	1	1	1
$\mathrm{SU}(2)_L$	2	1	1	2	1	1	2	2	1
$\mathrm{U}(1)_Y$	$\frac{1}{6}$	$+\frac{2}{3}$	$-\frac{1}{3}$	$-\frac{1}{2}$	-1	0	$+\frac{1}{2}$	$+\frac{1}{2}$	0
$\mathrm{U}(1)_R$	0	$+\frac{1}{2}$	$-\frac{1}{2}$	0	$-\frac{1}{2}$	$+\frac{1}{2}$	$q_1 = +\frac{1}{2}$	q_2	-1

Table 1. Matter contents and charge assignment of the model.

scalar field is also introduced. It plays an important role to reduce the mixing between left-handed neutrinos and the $\mathrm{U}(1)_R$ gauge boson, X, so that the stringent constraint from neutrino-electron scattering is avoided. The $\mathrm{U}(1)_R$ charge of H_2 is arbitrary, and we will discuss possible charge assignments later. The charge assignment of the new scalars is also shown in table 1, where we denote the $\mathrm{U}(1)_R$ charge of H_2 as q_2.

2.1 Lagrangian

The Lagrangian of the model takes the form of

$$\mathcal{L} = \mathcal{L}_{\text{fermion}} + \mathcal{L}_{\text{scalar}} + \mathcal{L}_{\text{gauge}} + \mathcal{L}_{\text{yukawa}} - V, \tag{2.1}$$

where each term denotes the fermion, scalar, gauge and Yukawa sector Lagrangian which are defined as

$$\mathcal{L}_{\text{fermion}} = i \sum_f \overline{f} \not{D} f, \tag{2.2a}$$

$$\mathcal{L}_{\text{scalar}} = |D_\mu H_1|^2 + |D_\mu H_2|^2 + |D_\mu S|^2, \tag{2.2b}$$

$$\mathcal{L}_{\text{gauge}} = -\frac{1}{4}\tilde{W}_{\mu\nu}\tilde{W}^{\mu\nu} - \frac{1}{4}\tilde{B}_{\mu\nu}\tilde{B}^{\mu\nu} - \frac{1}{4}\tilde{X}_{\mu\nu}\tilde{X}^{\mu\nu} + \frac{\epsilon}{2}\tilde{B}_{\mu\nu}\tilde{X}^{\mu\nu}, \tag{2.2c}$$

$$\mathcal{L}_{\text{yukawa}} = Y_u \overline{Q}\tilde{H}_1 u_R + Y_d \overline{Q} H_1 d_R + Y_e \overline{L} H_1 e_R d + Y_\nu \overline{L}\tilde{H}_1 N + Y_N \overline{N^c} S N + \text{h.c.} \tag{2.2d}$$

and V is the scalar potential which is given below. In eqs. (2.2), f represents the fermions (Q, u_L, u_R and L, e_R, N), and $\tilde{W}$, $\tilde{B}$ and $\tilde{X}$ represent the gauge fields and their field strengths in the interaction basis of $\mathrm{SU}(2)_L$, $\mathrm{U}(1)_Y$ and $\mathrm{U}(1)_R$, respectively. The covariant derivative in eqs. (2.2a) and (2.2b) is given by

$$D_\mu = \partial_\mu - i g_2 \tilde{W}_\mu - i Y g_1 \tilde{B} - i x g' \tilde{X}_\mu, \tag{2.3}$$

where Y and x represent the $\mathrm{U}(1)_Y$ and $\mathrm{U}(1)_R$ charges of each particle. The gauge coupling constants of $\mathrm{SU}(2)_L$, $\mathrm{U}(1)_Y$ and $\mathrm{U}(1)_R$ are denoted as g_2, g_1 and g', respectively. In eq. (2.2c), the gauge symmetry of the model allows the gauge kinetic mixing term between $\tilde{B}$ and $\tilde{X}$, and its magnitude is parameterized by the constant parameter ϵ. In eq. (2.2d), the Dirac Yukawa matrices are denoted as Y_u, Y_d and Y_e, Y_ν for up, down quarks and charged leptons, neutrinos, respectively. The Yukawa matrix for right-handed neutrinos is

JHEP04(2021)025

	q_2
Model 1	$-1/2$
Model 2	$+3/2$
Model 3	$-3/2$
Model 4	$+5/2$

Table 2. The charge assignments of H_2 for each model.

denoted as Y_N. Here $\tilde{H}_1$ represents $i\sigma_2 H_1^*$ where σ_2 is the Pauli matrix. Note that flavour and generation indices are omitted for simplicity.

The scalar potential V can be divided into two parts. One consists of the terms independent of the $\mathrm{U}(1)_R$ charge assignment of H_2, and the other consists of the terms dependent on that. The charge-independent part, V_0, is given by

$$\begin{aligned} V_0 = &-\mu_1^2|H_1|^2 - \mu_2^2|H_2|^2 - \mu_s^2|S|^2 + \frac{\lambda_1}{2}|H_1|^4 + \frac{\lambda_2}{2}|H_2|^4 + \frac{\lambda_s}{2}|S|^4 \\ &+ \lambda_1'|H_1^\dagger H_2|^2 + \lambda_2'|H_1|^2|H_2|^2 + \lambda_3'|S|^2|H_1|^2 + \lambda_4'|S|^2|H_2|^2, \end{aligned} \tag{2.4}$$

where we assume the mass parameters as well as the quartic couplings to be positive so that spontaneous breaking of the symmetries successfully occurs, and no runaway directions appear in the potential. With the above potential, we obtain five Nambu-Goldstone bosons after H_1, H_2 and S develop vacuum expectation values (VEVs). Two of those are absorbed by the charged weak boson, $W^\pm$, and other two are absorbed by the neutral weak boson Z and the new gauge boson, $\tilde{X}$. Then, one massless CP-odd scalar remains in the spectrum, which corresponds to the broken degree of freedom of the phase rotation of H_2. Such a massless scalar boson causes serious problems by carrying the energy of stars and conflicts with meson decay measurement such as an axion does [45, 46]. Therefore we need to introduce other interaction terms which give the mass to the CP-odd scalar after the symmetry breaking. In this sense, a possible choice of q_2 is determined. We classify models with different choices of q_2 given in table 2.

The charge-dependent scalar potential in each model is given by

$$\text{Model 1}: \quad \Delta V_1 = A_1 S H_2^\dagger H_1 + \text{h.c.}, \tag{2.5a}$$

$$\text{Model 2}: \quad \Delta V_2 = A_2 S H_1^\dagger H_2 + \text{h.c.}, \tag{2.5b}$$

$$\text{Model 3}: \quad \Delta V_3 = \kappa_1 S^2 H_2^\dagger H_1 + \text{h.c.}, \tag{2.5c}$$

$$\text{Model 4}: \quad \Delta V_4 = \kappa_2 S^2 H_1^\dagger H_2 + \text{h.c.}, \tag{2.5d}$$

where the parameters, $A_{1,2}$ and $\kappa_{1,2}$, can be taken real by using phase rotation of H_2. One example of the parameter sets to reproduce the Higgs mass, 125 GeV, for Model 1 is found as

$$\begin{aligned} &v = 246.0 \text{ GeV}, && v_s = 2v, && \cos 2\beta = 0 \ \ (\tan\beta = 1), \\ &\lambda_1 = 1.19, && \lambda_2 = 1.2, && \lambda_1' = \lambda_2' = 0, \\ &\lambda_s = \lambda_3' = \lambda_4' = 5.0, \\ &A_1 = -\sqrt{2}\lambda_3' \tan\beta v_s + 938 \text{ GeV}, \end{aligned} \tag{2.6}$$

JHEP04(2021)025

With these parameters, the masses of the CP-even (h_1, h_2, h_3), CP-odd (a) and charged Higgs $(h^\pm)$ bosons are given by

$$\begin{aligned} m_{h_1} &= 125.5 \text{ GeV}, & m_{h_2} &= 1158.1 \text{ GeV}, & m_{h_3} &= 1343.2 \text{ GeV}, \\ m_a &= 1370.6 \text{ GeV}, & m_{h^\pm} &= 1329.7 \text{ GeV}, \end{aligned} \tag{2.7}$$

where h_2 is singlet-like and other scalar bosons are doublet-like. The couplings of h_1 to the weak gauge bosons are almost the same as those of the SM ($\sin\beta U_{h_1H_1} + \cos\beta U_{h_1H_2} \simeq 0.992$ with $U_{h_1H_1}$ and $U_{h_1H_2}$ being the components of H_1 and H_2 in h_1), and that of h_1 to the X bosons is much suppressed by a tiny component ($\sin\beta U_{h_1H_1} + \cos\beta U_{h_1H_2} + 4\frac{v_s}{v} U_{h_1S} \simeq 1.9 \times 10^{-4}$ with U_{h_1S} being the components of S in h_1). The searches for exotic decays of the SM Higgs boson $h_1 \to XX \to 4e$ have been done in [47], however, the mass range of the X boson is restricted as $> 15\,\text{GeV}$ in the analysis. Therefore, the gauge boson lighter than 15 GeV is not constrained by the four lepton search. When such an exotic decay is identified as invisible decays at LHC, the present bound on the invisible branching ratio is given by 0.26 at 95% C.L. [48]. The decay branching ratio of $h_1 \to XX$ for the X boson with 17 MeV mass is about 1.3×10^{-5} which is much smaller than the bound. For the decays and productions of h_1 in the SM processes, the predictions of our model are $\kappa_f \equiv Y_f v/m_f \simeq 0.996$ and $\sqrt{\kappa_V} \equiv g_V v/m_V \simeq 0.985$ where f and V represent fermions and weak gauge bosons, and g_V is the coupling constant for V, respectively. Those are consistent with the latest results of combined analyses shown in figure 12 of [49].

The singlet-like scalar boson h_2 could be produced at LHC. Once produced, it decays into XX dominantly. Although the X boson itself has not been searched, its decay into an electron-positron pair could potentially be mis-reconstructed as a photon [50, 51]. Diphoton events from new heavy particles have been searched at LHC and the constraints are given as $\lesssim 1\,\text{fb}$ in [52, 53]. From the parameters given in eq. (2.6), the coupling of h_2 to top quark is suppressed by 0.12 to the SM one. Then, the signal cross section is estimated as at most 0.45 fb with converted decay probability given in [51]. Hence this constraint also can be evaded. The present lower bounds on the masses of the doublet-like heavy CP even, odd, and charged Higgs boson are 490 GeV for $\cos(\beta-\alpha) = -0.1$ and $\tan\beta = 1$ [54] , 300 GeV [55] and 600 GeV [56] for $\tan\beta = 1$, respectively. The mass spectrum and the value of $\cos(\beta-\alpha)$ in our above sample point, eq. (2.7), is consistent with the latest bound. Furthermore, the present bounds from Higgs measurements and electroweak precision measurements also can be evaded due to the degenerate masses of the heavy Higgs bosons [57, 58].

Details of the scalar sector are essentially irrelevant to our study about the Atomki anomaly. One exceptional issue relevant to the detail of the Higgs sector, especially charged Higgs scalars, is flavour changing meson decays with radiating the longitudinal mode of the X boson such as $K \to \pi X$, $B \to KX$ via a charged Higgs boson loop. It was pointed out in [59, 60] that such decays in a $\text{U}(1)_R$ model [61] are indeed enhanced, and the constraints from these show a tension with the Atomki signal, unless all of the decay modes are suppressed by fine-tunings. An extension of the Higgs sector could provide such tunings for all decay modes. However, such an extension is beyond the scope of this paper, and left for our future work. In this paper, we focus on the gauge sector which is most

JHEP04(2021)025

relevant to the Atomki signal, and assume that the parameters in the scalar potential are appropriately chosen so that the new gauge boson acquires the mass required to explain the Atomki anomaly.

2.2 Gauge boson masses and mass eigenstates

After the EW and $\mathrm{U}(1)_R$ symmetries are broken down, the gauge boson masses are generated via the VEVs of the scalar fields. We denote the VEVs as

$$\langle H_1\rangle = \frac{1}{\sqrt{2}}\begin{pmatrix}0\\ v_1\end{pmatrix}, \quad \langle H_2\rangle = \frac{1}{\sqrt{2}}\begin{pmatrix}0\\ v_2\end{pmatrix}, \quad \langle S\rangle = \frac{1}{\sqrt{2}}v_s, \tag{2.8}$$

and each scalar field is expanded around its VEV as

$$H_1 = \begin{pmatrix}\hat{H}_1^+\\ \frac{1}{\sqrt{2}}(v_1+\hat{h}_1+i\hat{a}_1)\end{pmatrix}, \quad H_2 = \begin{pmatrix}\hat{H}_2^+\\ \frac{1}{\sqrt{2}}(v_2+\hat{h}_2+i\hat{a}_2)\end{pmatrix}, \quad S = \frac{1}{\sqrt{2}}(v_s+\hat{s}+i\hat{\zeta}). \tag{2.9}$$

Then, the mass terms of the gauge fields are given by

$$\mathcal{L}_{\text{gauge,mass}} = \frac{1}{8}\sum_{i=1}^{2} v_i^2\left[2g_2^2 W_\mu^+ W^{-\mu} + \left(-\sqrt{g_1^2+g_2^2}\tilde{Z}_\mu + 2q_i g'\tilde{X}_\mu\right)^2\right] + \frac{1}{2}g'^2 v_s^2 \tilde{X}_\mu\tilde{X}^\mu, \tag{2.10}$$

with

$$W_\mu^\pm = \frac{1}{\sqrt{2}}(\tilde{W}_\mu^1 \mp i\tilde{W}_\mu^2), \tag{2.11a}$$

$$\tilde{Z}_\mu = \cos\theta_W \tilde{W}_\mu^3 - \sin\theta_W \tilde{B}_\mu, \tag{2.11b}$$

$$\tilde{A}_\mu = \sin\theta_W \tilde{W}_\mu^3 + \cos\theta_W \tilde{B}_\mu. \tag{2.11c}$$

Here, θ_W is the Weinberg angle of the SM defined by $\sin\theta_W = g_1/\sqrt{g_1^2+g_2^2}$. The gauge boson, $W^\pm$, is the charged weak gauge boson of the SM, and $\tilde{Z}$ and $\tilde{A}$ correspond to the Z boson and photon in the SM limit, $(g', \epsilon) \to 0$. In the following, we parameterize the VEVs as,

$$v_1 = v\sin\beta, \;\; v_2 = v\cos\beta, \;\; v^2 = v_1^2 + v_2^2. \tag{2.12}$$

With this parametrization, the charged weak gauge boson mass is given by

$$m_W = \frac{g_2}{2}v. \tag{2.13}$$

The mass terms of the neutral gauge bosons can be casted in a 3×3 matrix as

$$\mathcal{L}_{\text{mass}} = \frac{1}{2}\tilde{F}_\mu^T m_{\tilde{F}}^2 \tilde{F}^\mu, \tag{2.14}$$

where $\tilde{F}_\mu = (\tilde{A}_\mu, \tilde{Z}_\mu, \tilde{X}_\mu)^T$, and $m_{\tilde{F}}^2$ is given by

$$m_{\tilde{F}}^2 = \begin{pmatrix}0 & 0 & 0\\ 0 & m_{\tilde{Z}}^2 & -g'vm_{\tilde{Z}}(q_1\sin^2\beta + q_2\cos^2\beta)\\ 0 & -g'vm_{\tilde{Z}}(q_1\sin^2\beta+q_2\cos^2\beta) & g'^2v_s^2 + g'^2v^2(q_1^2\sin^2\beta + q_2^2\cos^2\beta)\end{pmatrix}. \tag{2.15}$$

JHEP04(2021)025

Here, $m_{\tilde{Z}}$ is the SM Z boson mass defined by

$$m_{\tilde{Z}} = \frac{1}{2}\sqrt{g_1^2 + g_2^2}v. \tag{2.16}$$

To obtain the masses of the neutral gauge bosons, we first diagonalize the gauge boson kinetic term by changing the basis of the fields $\tilde{F}$ to $\overline{F} = (\overline{A}, \overline{Z}, \overline{X})^T$ as

$$\tilde{F} = U_K \overline{F}, \tag{2.17}$$

where U_K is an orthogonal matrix given by

$$U_K = \begin{pmatrix} 1 & 0 & \epsilon r \cos\theta_W \\ 0 & 1 & -\epsilon r \sin\theta_W \\ 0 & 0 & r \end{pmatrix}, \tag{2.18}$$

with $r = (1-\epsilon^2)^{-1/2}$. Then, the mass matrix in the $\overline{F}_\mu$ basis is given as

$$m_{\overline{F}}^2 = U_K^T m_{\tilde{F}}^2 U_K = \begin{pmatrix} 0 & 0 & 0 \\ 0 & m_{\tilde{Z}}^2 & -r m_{\tilde{Z}} \delta_1 \\ 0 & -r m_{\tilde{Z}} \delta_1 & r^2(g'^2 v_s^2 + \delta_1^2 + \delta_2^2) \end{pmatrix}, \tag{2.19}$$

with

$$\delta_1 = \epsilon \sin\theta_W m_{\tilde{Z}} + g' v (q_1 \sin^2\beta + q_2 \cos^2\beta), \tag{2.20}$$

$$\delta_2 = |g' v (q_1 - q_2) \sin\beta \cos\beta|. \tag{2.21}$$

Next, the mass matrix eq. (2.19) can be diagonalized by an orthogonal matrix V_F

$$\overline{F} = V_F F, \tag{2.22a}$$

$$V_F = \begin{pmatrix} 1 & 0 & 0 \\ 0 & \cos\chi & -\sin\chi \\ 0 & \sin\chi & \cos\chi \end{pmatrix}, \tag{2.22b}$$

where $F = (A, Z, X)^T$ is the mass eigenstates. Their mass eigenvalues are given by

$$m_A^2 = 0, \tag{2.23a}$$

$$m_Z^2 = m_{\tilde{Z}}^2 \cos^2\chi + r^2(g'^2 v_s^2 + \delta_1^2 + \delta_2^2)\sin^2\chi - 2 r m_{\tilde{Z}} \delta_1 \sin\chi\cos\chi, \tag{2.23b}$$

$$m_X^2 = r^2(g'^2 v_s^2 + \delta_1^2 + \delta_2^2)\cos^2\chi + m_{\tilde{Z}}^2 \sin^2\chi + 2 r m_{\tilde{Z}} \delta_1 \sin\chi\cos\chi. \tag{2.23c}$$

The mixing angle χ can be expressed as

$$\tan\chi = -\frac{r m_{\tilde{Z}} \delta_1}{m_{\tilde{Z}}^2 - m_X^2}. \tag{2.24}$$

Here the mass of X is an input of the model which should be $\simeq 17\,\mathrm{MeV}$ by the Atomki experiment. In the situation of $m_{\tilde{Z}} \gg m_X$, the leading term of eq. (2.24) is given by

$$\tan\chi \simeq -r\epsilon \sin\theta_W - r\frac{g' v}{m_{\tilde{Z}}}(q_1 \sin^2\beta + q_2 \cos^2\beta). \tag{2.25}$$

JHEP04(2021)025

In the parameter space of our interest, g' and ϵ are roughly $\mathcal{O}(10^{-4} - 10^{-3})$. Therefore, χ is much smaller than unity from eq. (2.25). Then, the difference between m_Z and $m_{\tilde{Z}}$ is roughly given as,

$$m_Z^2 - m_{\tilde{Z}}^2 \simeq \delta_1^2 \simeq \max(\epsilon^2 m_{\tilde{Z}}^2, g'^2 v^2) \sim (100\ \text{MeV})^2, \tag{2.26}$$

where eq. (2.23b) is used. This difference is smaller than the present error of the measured Z boson mass, $91.1876 \pm 0.0021\,\text{GeV}$ [62] and therefore we use $m_{\tilde{Z}} \simeq m_Z = 91.1876\,\text{GeV}$ as an input value in the following discussion. Then, v_s is expressed in terms of other parameters as

$$v_s^2 = \frac{m_X^2(m_Z^2 + r^2(\delta_1^2 + \delta_2^2)) - r^2 m_Z^2 \delta_2^2 - m_X^4}{r^2 g'^2 (m_Z^2 - m_X^2)}. \tag{2.27}$$

Right-hand-side of eq. (2.27) should be positive for consistency.

In the end, the gauge eigenstates are expressed in terms of the mass eigenstates as

$$\begin{pmatrix} \tilde{A}_\mu \\ \tilde{Z}_\mu \\ \tilde{X}_\mu \end{pmatrix} = U \begin{pmatrix} A_\mu \\ Z_\mu \\ X_\mu \end{pmatrix} = \begin{pmatrix} A_\mu + U_{12} Z_\mu + U_{13} X_\mu \\ U_{22} Z_\mu + U_{23} X_\mu \\ U_{32} Z_\mu + U_{33} X_\mu \end{pmatrix}, \tag{2.28}$$

where $U = U_K V_F$ and its elements are

$$U_{12} = \epsilon r \cos\theta_W \sin\chi, \qquad U_{13} = \epsilon r \cos\theta_W \cos\chi, \tag{2.29a}$$

$$U_{22} = \cos\chi - \epsilon r \sin\theta_W \sin\chi, \qquad U_{23} = -\sin\chi - \epsilon r \sin\theta_W \cos\chi, \tag{2.29b}$$

$$U_{32} = r \sin\chi, \qquad U_{33} = r \cos\chi. \tag{2.29c}$$

From eqs. (2.11) and (2.28), the Lagrangian can be written in the mass basis of the gauge boson.

3 Couplings of the X boson to fermions

In this section, we present the coupling constants of the X boson to quarks and leptons. The gauge interactions of the fermions to the X boson are modified due to the mixing among the gauge bosons. Using eqs. (2.11) and (2.28) with eqs. (2.29), the interaction Lagrangian of fermions, f $(= u, d, \nu, N)$, can be written in the following form,

$$\mathcal{L}_{\text{int}} = e \overline{f} \gamma^\mu (\epsilon_f^V + \epsilon_f^A \gamma^5) f X_\mu, \tag{3.1}$$

where e is the proton electric charge. The vector coupling ϵ_f^V and axial-vector couplings ϵ_f^A are given by

$$\epsilon_u^V = \frac{1}{4}\epsilon_R r \cos\chi + \frac{2}{3}\epsilon r \cos\theta_W \cos\chi - \left(\frac{1}{4} - \frac{2}{3}\sin^2\theta_W\right)\epsilon_{\text{NC}}, \tag{3.2a}$$

$$\epsilon_u^A = \frac{1}{4}\epsilon_R r \cos\chi + \frac{1}{4}\epsilon_{\text{NC}}, \tag{3.2b}$$

JHEP04(2021)025

$$\epsilon_d^V = -\frac{1}{4}\epsilon_R r\cos\chi - \frac{1}{3}\epsilon r\cos\theta_W\cos\chi + \left(\frac{1}{4} - \frac{1}{3}\sin^2\theta_W\right)\epsilon_{\rm NC}, \tag{3.2c}$$

$$\epsilon_d^A = -\epsilon_u^A = \epsilon_e^A = -\frac{1}{4}\epsilon_R r\cos\chi - \frac{1}{4}\epsilon_{\rm NC}, \tag{3.2d}$$

$$\epsilon_e^V = -\frac{1}{4}\epsilon_R r\cos\chi - \epsilon r\cos\theta_W\cos\chi + \left(\frac{1}{4} - \sin^2\theta_W\right)\epsilon_{\rm NC}, \tag{3.2e}$$

$$\epsilon_\nu^V = -\epsilon_\nu^A = -\frac{1}{4}\epsilon_{\rm NC}, \quad \epsilon_N^V = \epsilon_N^A = \frac{1}{4}\epsilon_R r c_\chi, \tag{3.2f}$$

with $\epsilon_R = g'/e$, where $\epsilon_{\rm NC}$ represents the neutral current contribution defined by

$$\epsilon_{\rm NC} = \frac{\sin\chi + \epsilon r\sin\theta_W\cos\chi}{\sin\theta_W\cos\theta_W}. \tag{3.3}$$

In eqs. (3.2), we neglect the mixing between left and right handed neutrinos.[2] As we explained above, one of the most stringent constraints comes from neutrino-electron scattering of reactor neutrinos measured at TEXONO [63]. The left-handed neutrinos ν_L can interact with the X boson through the weak neutral current. Thus, the coupling constant of ν_L is proportional to $\epsilon_{\rm NC}$ as

$$\epsilon_{\nu_L} = -\frac{1}{2}\epsilon_{\rm NC}. \tag{3.4}$$

To obtain approximate formulae of the coupling constants, we expand $\epsilon_{\rm NC}$ in the limit of $|\chi| \ll 1$ and $|Q| \ll 1$ as,

$$\begin{aligned}\epsilon_{\rm NC} &\simeq -\frac{m_{\tilde{Z}}^2 Q\epsilon_R\cos\theta_W + \epsilon m_X^2}{\cos\theta_W(m_{\tilde{Z}}^2 - m_X^2)} \\ &\simeq -Q\epsilon_R - \left(Q\epsilon_R + \frac{\epsilon}{\cos\theta_W}\right)\frac{m_X^2}{m_{\tilde{Z}}^2} + \mathcal{O}\left(Q\epsilon_R\frac{m_X^4}{m_{\tilde{Z}}^4},\ \frac{\epsilon}{\cos\theta_W}\frac{m_X^4}{m_{\tilde{Z}}^4}\right),\end{aligned} \tag{3.5}$$

where we define Q for convenience as

$$Q = (q_1 + q_2) - (q_1 - q_2)\cos 2\beta. \tag{3.6}$$

In the expansion, we kept the leading term of ϵ and ϵ_R and neglected higher order terms of these couplings in each power of $m_X^2/m_{\tilde{Z}}^2$. Inserting eq. (3.5) into eqs. (3.2), the approximate expression of the coupling constants can be obtained, which is useful to understand signal requirement and constraints as we will explain later.

The first term of eq. (3.5) vanishes when β takes a specific value of

$$\cos 2\beta^* \equiv \frac{q_1 + q_2}{q_1 - q_2}. \tag{3.7}$$

Then, the remaining term is much smaller than ϵ due to $m_{\tilde{Z}} \gg m_X$. From table 2, $\cos 2\beta^*$ is given in each Model by

$$\text{Model 1}: \quad \cos 2\beta^* = 0, \tag{3.8a}$$

$$\text{Model 2}: \quad \cos 2\beta^* = -2, \tag{3.8b}$$

[2]The mixing between the left and right-handed neutrinos is roughly given by $\sqrt{\frac{m_\nu}{M}}$ where m_ν and M are the active neutrino mass and Majorana mass, respectively. Taking $Y_N = \mathcal{O}(1)$, The Majorana mass is $\mathcal{O}(v_s)$ and larger than 10 GeV for $g' < 10^{-3}$. Thus, the mixing is smaller than 10^{-4} for $m_\nu \sim 0.1$ eV.

JHEP04(2021)025

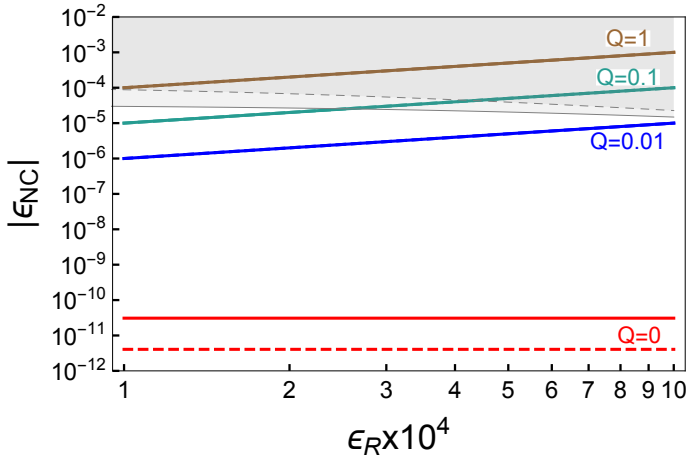

Figure 1. The coupling $\epsilon_{\rm NC}$ as a function of ϵ_R. Red, blue, green and brown lines correspond to $Q = 0,\ 0.01,\ 0.1$ and 1, respectively. Solid and dashed ones correspond to $\epsilon = 5 \times 10^{-4}$ and 10^{-4}. Gray filled region are exclusion region by the TEXONO results.

$$\text{Model 3}: \quad \cos 2\beta^* = -\frac{1}{2}, \tag{3.8c}$$

$$\text{Model 4}: \quad \cos 2\beta^* = -\frac{3}{2}. \tag{3.8d}$$

Thus, Q can be vanished in Model 1 and 3, while there are no solutions for $Q = 0$ in Model 2 and 4. Figure 1 is a plot of $|\epsilon_{\rm NC}|$ as a function of ϵ_R. Red, blue, green and brown lines correspond to $Q = 0,\ 0.01,\ 0.1$ and 1, respectively. Solid and dashed ones correspond to $\epsilon = 10^{-4}$ and 5×10^{-4}. Gray filled regions with solid and dashed edges are exclusion region by neutrino-electron scattering for $\epsilon = 5 \times 10^{-4}$ and 10^{-4}, which we will explain in subsection 4.2.2.[3] Except for $Q = 0$, the dashed and solid curves are almost the same. One can see that the allowed region exists for $Q \leq 0.1$ while it does not for $Q \geq 1$. Thus, Model 1 and 3 can evade the constraint from the ν-e scattering while Model 2 and 4, with $Q \geq 1$, are excluded for the choice of the parameters. When $Q \leq 0.01$, the constraint can be evaded in the region of ϵ_R of our interest in Model 1 and 3. In this case, $\tan\beta$ should be tuned to the value obtained from (3.7) more than 1 %, which is calculated from

$$\frac{\tan\beta - \tan\beta^*}{\tan\beta^*} \simeq Q\ \left(\frac{2}{3}Q\right), \tag{3.9}$$

for Model 1 (3).

4 Signal and experimental constraints

We summarize the signal requirement from the ^{8}Be decay[4] and the constraints from various experiments.

[3]It should be noted that the exclusion region in ϵ_R-$\epsilon_{\rm NC}$ plane is almost independent of Q. In figure, we fixed $Q = 0$.

[4]As we explained in the Introduction, the Atomki collaboration also reported that a peak like excess was found in ^{4}He [6], which can be consistently explained by a light particle for ^{8}Be . However, nuclear matrix elements have significant uncertainty for ^{4}He [35] and we need further study to reduce the uncertainty. Thus we will not indicate ^{4}He anomaly in our analysis.

JHEP04(2021)025

	Previous Result [1]	Exp1	Exp2	Average
m_X (MeV)	16.70(51)	16.86(6)	17.17(7)	17.01(16)
B_X ($\times 10^{-6}$)	5.8	6.8(10)	4.7(21)	6(1)
Significance	6.8σ	7.37σ	4.90σ	

Table 3. The mass of X particle and branching ratio of ^{8}Be* .

4.1 Signal requirement

4.1.1 ^{8}Be* decay branching ratio

The Atomki collaboration has reported an anomalous internal pair creation for the M1 transition of the 18.15 MeV excited state ^{8}Be* of ^{8}Be [1–5]. The collaboration measured angular correlations, and found a significant peak-like enhancement at larger angles. This result is mostly well-fitted under the assumption of the creation and subsequent decay of an intermediate particle X with a mass of

$$m_X \simeq 17.0 \text{ MeV}. \tag{4.1}$$

The signal branching ratio of ^{8}Be* into the assumed X particle, followed by the decay of X into e^+e^-, is defined by

$$B_X \equiv \frac{\Gamma(^8\text{Be}^* \to {}^8\text{Be}X)}{\Gamma(^8\text{Be}^* \to {}^8\text{Be}\gamma)} \text{Br}(X \to e^+e^-), \tag{4.2}$$

where $\Gamma(^8\text{Be}^* \to {}^8\text{Be}\gamma) \simeq (1.9 \pm 0.4)\,\text{eV}$ is the partial width of the γ decay of ^{8}Be* and $\text{Br}(X \to e^+e^-)$ is the decay branching ratio of X into an electron-positron pair. From the Atomki experiment, the branching ratio (4.2) and the X boson mass have been constrained as given in table 3 (taken from [5]). These values have a relatively large uncertainty, which may originate from systematic uncertainty of unstable beam position in the experiment. Therefore, we employ a rather conservative range for our numerical calculation

$$4 \times 10^{-7} \lesssim B_X \lesssim 7 \times 10^{-6}, \tag{4.3}$$

where m_X is taken to 17.6 and 16.7 MeV for the lower and upper bounds, respectively.

To calculate the decay branching ratio of ^{8}Be*, we employ the results given in [30]. The partial decay width from the axial part of the gauge interaction is expressed as

$$\Gamma(^8\text{Be}^* \to {}^8\text{Be}X) = \frac{k}{18\pi}\left(2 + \frac{E_k^2}{m_X^2}\right)\left|a_n\langle 0||\sigma^n||1\rangle + a_p\langle 0||\sigma^p||1\rangle\right|^2, \tag{4.4}$$

where $k = \sqrt{\Delta E^2 - m_X^2}$ and $E_k = \Delta E$ are the three momentum and energy of the X boson, with $\Delta E = 18.15\,\text{MeV}$ being the difference of the energy level. The proton and neutron couplings, a_p and a_n, are defined as

$$a_p = \frac{a_0 + a_1}{2}, \tag{4.5a}$$

$$a_n = \frac{a_0 - a_1}{2}, \tag{4.5b}$$

JHEP04(2021)025

where

$$a_0 = (\Delta u^{(p)} + \Delta d^{(p)})(\epsilon_u^A + \epsilon_d^A) + 2\Delta s^{(p)}\epsilon_d^A = 2\Delta s^{(p)}\epsilon_d^A, \tag{4.6a}$$

$$a_1 = (\Delta u^{(p)} - \Delta d^{(p)})(\epsilon_u^A - \epsilon_d^A) = 2(\Delta u^{(p)} - \Delta d^{(p)})\epsilon_u^A, \tag{4.6b}$$

and $\epsilon_{u,d}^A$ is given in eqs. (3.2). The quark coefficients take values [64]

$$\Delta u^{(p)} = \Delta d^{(n)} = \quad 0.897(27), \tag{4.7a}$$

$$\Delta d^{(p)} = \Delta u^{(n)} = -0.367(27), \tag{4.7b}$$

$$\Delta s^{(p)} = \Delta s^{(n)} = -0.026(4), \tag{4.7c}$$

and the nuclear matrix elements takes [30]

$$\langle 0^+ \| \sigma^p \| \mathcal{S} \rangle = -0.047(29), \tag{4.8a}$$

$$\langle 0^+ \| \sigma^n \| \mathcal{S} \rangle = -0.132(33). \tag{4.8b}$$

Inserting eq. (4.4) with these numbers into eq. (4.2), we obtain the branching ratio of ^{8}Be* decay.

Before closing this subsection, we show the parameter dependence of the signal branching ratio. Using $\epsilon_d^A = -\epsilon_u^A = \epsilon_e^A$, the partial decay width of ^{8}Be* is proportional to $(\epsilon_e^A)^2$ as

$$\Gamma(^8\mathrm{Be}^* \to {}^8\mathrm{Be}X) \propto \frac{k}{18\pi}\left(2 + \frac{E_k^2}{m_X^2}\right)(\epsilon_e^A)^2. \tag{4.9}$$

The decay branching ratio of $X \to e^+e^-$ is given by

$$\mathrm{Br}(X \to e^+e^-) = \frac{\epsilon_e^{V\,2} + \epsilon_e^{A\,2}}{\epsilon_e^{V\,2} + \epsilon_e^{A\,2} + \frac{3}{2}\epsilon_{\nu_L}^2}, \tag{4.10}$$

where $\epsilon_e^{V,A}$ and ϵ_{ν_L} are given in eqs. (3.2) and (3.4). In eq. (4.10), we have neglected the masses of electron and neutrino. In the case of $|\chi| \ll 1$ and $|Q| \ll 1$, ϵ_e^A can be approximated as

$$\epsilon_e^A \simeq -\frac{1}{4}(1-Q)\epsilon_R + \frac{1}{4}\left(Q\epsilon_R + \frac{\epsilon}{\cos\theta_W}\right)\frac{m_X^2}{m_{\tilde{Z}}^2}, \tag{4.11}$$

where eq. (3.5) is used. Similarly, the vector coupling of electron is approximated as

$$\begin{aligned}\epsilon_e^V \simeq & -\frac{1}{4}(1 + (1 - 4\sin^2\theta_W)Q)\epsilon_R - \cos\theta_W\epsilon \\ & - \left(\frac{1}{4} - \sin^2\theta_W\right)\left(Q\epsilon_R + \frac{\epsilon}{\cos\theta_W}\right)\frac{m_X^2}{m_{\tilde{Z}}^2},\end{aligned} \tag{4.12}$$

Thus, neglecting $\mathcal{O}(m_X^2/m_{\tilde{Z}}^2)$ terms, the branching ratio, eq. (4.10), is expressed by

$$\mathrm{Br}(X \to e^+e^-) \simeq 1 - \frac{3}{2}\frac{4Q^2\epsilon_R^2}{(\epsilon_R + 4\cos\theta_W\epsilon)^2 + \epsilon_R^2}. \tag{4.13}$$

JHEP04(2021)025

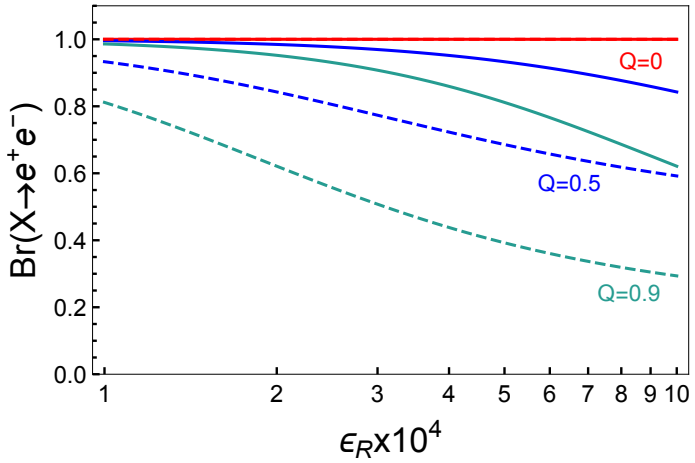

Figure 2. The branching ratio of $X \to e^+e^-$ as a function of ϵ_R. Red, blue and green curves correspond to $Q = 0,\ 0.5$ and 0.9, respectively. Solid and dashed ones correspond to $\epsilon = 5 \times 10^{-4}$ and 10^{-4}.

Figure 2 shows the branching ratio of $X \to e^+e^-$ as a function of ϵ_R. We fixed as $\epsilon = 5 \times 10^{-4}$ (solid) and 10^{-4} (dashed) and as $Q = 0$ (red), 0.5 (blue) and 0.9 (green), respectively. One can see that the branching ratio decrease as Q increases. This is because the coupling to neutrinos, which is proportional to $\epsilon_{\rm NC}$, becomes large for non-vanishing Q as shown in figure 1.

Using the approximate expressions, eqs. (4.11) and (4.13), the signal branching ratio is scaled by the parameters as

$$\begin{aligned} B_X &\propto (\epsilon_e^A)^2 \frac{\epsilon_e^{V\,2} + \epsilon_e^{A\,2}}{\epsilon_e^{V\,2} + \epsilon_e^{A\,2} + \frac{3}{2}\epsilon_{\nu_L}^2} \\ &\propto (1-Q)^2 \epsilon_R^2 \left[1 - \frac{3}{2} \frac{4Q^2\epsilon_R^2}{(\epsilon_R + 4\cos\theta_W \epsilon)^2 + \epsilon_R^2}\right]. \end{aligned} \tag{4.14}$$

Thus, for $|Q| \ll 1$, the branching ratio is simply determined by $(\epsilon_R)^2$.

4.1.2 *X* boson lifetime

To explain the Atomki anomaly, the new vector should decay inside the detector so that the electro-positron pair can be detected. As in [10], we require that the X boson propagates less than 1 cm from its production point, which gives the condition as

$$\sqrt{(\epsilon_e^V)^2 + (\epsilon_e^A)^2} \geq 1.3 \times 10^{-5} \sqrt{{\rm Br}(X \to e^+e^-)}. \tag{4.15}$$

4.2 Constraints

4.2.1 Rare decay of neutral pion

The coupling constants of the light gauge boson to quarks can be constrained by meson decay experiments. The gauge boson can be produced in rare meson decays when those are kinematically allowed. For the X boson with $m_X \simeq 17\,{\rm MeV}$, the most stringent constraint

JHEP04(2021)025

among such meson decays comes from the rare decay of neutral pion into X with a photon, i.e. $\pi^0 \to \gamma X$. Theoretically, only vectorial parts of the X interaction to quarks can contribute to the decay. The latest result of the NA48/2 experiment [65] puts the following bound,

$$|2\epsilon_u^V + \epsilon_d^V| \leq \frac{0.3 \times 10^{-3}}{e\sqrt{\mathrm{Br}(X \to e^+e^-)}}. \tag{4.16}$$

The left-hand-side of the constraint is rewritten by

$$2\epsilon_u^V + \epsilon_d^V = -\epsilon_e^V, \tag{4.17}$$

and approximated as eq. (4.12). For $|Q| \ll 1$, eq. (4.16) is simplified as

$$\left|\frac{1}{4}\epsilon_R + \cos\theta_W \epsilon\right| \leq 10^{-3}. \tag{4.18}$$

4.2.2 Neutrino-electron scattering

The interaction of the gauge boson to leptons, especially to neutrinos, is tightly constrained by neutrino-electron scattering [66]. The most stringent constraint for the X boson is given by the TEXONO experiment [67]. In [67], the contributions from the $B-L$ gauge boson to $\overline{\nu_e}$-e scattering have been studied. The authors analyzed the differential cross section with respect to the recoil energy of scattered electron and showed the interference term gives sizable contributions. Based on the analyses, the allowed region of the mass and gauge coupling of the $B-L$ gauge boson was shown. In this work, we derive the interference term of the differential cross section in the $\mathrm{U}(1)_R$ model, and constrain the parameters by comparing the differential cross section in the SM.[5]

The differential cross section in the SM and the interference term between the SM and X boson contributions are given by

$$\left(\frac{d\sigma}{dT}\right)_{\mathrm{SM}} = \frac{2m_e G_F^2}{\pi E_\nu^2}(g_R^2 E_\nu^2 + g_L^2(E_\nu - T)^2 - g_L g_R m_e T), \tag{4.19a}$$

$$\left(\frac{d\sigma}{dT}\right)_{\mathrm{int}} = \frac{g'_\nu m_e G_F}{\sqrt{2}\pi(m_X^2 + 2m_e T)}(2g_R g'_L E_\nu^2 + 2g_L g'_R(E_\nu - T)^2 - (g_L g'_R + g_R g'_L)m_e T), \tag{4.19b}$$

where T and m_e are the recoil energy and the mass of electron, and E_ν is the energy of incident neutrino, respectively. The Fermi constant is denoted as G_F, and other coupling constants are given by

$$g_L = \frac{1}{2} + \sin^2\theta_W, \qquad g_R = \sin^2\theta_W, \tag{4.20a}$$

$$g'_L = e(\epsilon_e^V - \epsilon_e^A), \qquad g'_R = e(\epsilon_e^V + \epsilon_e^A), \tag{4.20b}$$

$$g'_\nu = 2e\epsilon_\nu^V. \tag{4.20c}$$

[5] Recently, in [20], this constraint is computed using data and χ^2 fit is performed. As we have shown in figure 1, the coupling constant of neutrinos is much smaller than 10^{-5} for small Q. Therefore, our result is consistent with that of [20].

JHEP04(2021)025

From [63], the event rate relative to that of the SM is given by $1.08 \pm 0.21(\text{stat}) \pm 0.16(\text{sys})$ in the TEXONO experiment. Thus we require

$$-0.64 < \frac{\left(\frac{d\sigma}{dT}\right)_{\text{int}}}{\left(\frac{d\sigma}{dT}\right)_{\text{SM}}} < 0.8, \tag{4.21}$$

which corresponds to 3σ range. We use our numerical analysis $E_\nu = 3.0\,\text{MeV}$ and $T = 3.0\,\text{MeV}$, respectively.

The ratio in eq. (4.21) can be approximated for the case of $|\chi| \ll 1$ and $|Q| \ll 1$ as,

$$\frac{\left(\frac{d\sigma}{dT}\right)_{\text{int}}}{\left(\frac{d\sigma}{dT}\right)_{\text{SM}}} \simeq -(5.0 \times 10^7 Q + 1.3)\epsilon\epsilon_R. \tag{4.22}$$

It can be understood from above equation that Q is important for this constraint. Unless Q is very close to zero, the constraint excludes $\epsilon\epsilon_R \gtrsim 10^{-8}/Q$.

4.2.3 Anomalous magnetic moment of charged lepton

The anomalous magnetic moments of the charged leptons have been measured accurately by experiments and also predicted precisely in the SM. The new vector boson, that couples to the charged leptons, can shift the anomalous magnetic moments from the SM predictions via quantum loop corrections. One loop contribution of the vector boson is given by [68]

$$\delta a_l = \frac{e^2}{4\pi^2}\left((\epsilon_l^V)^2 I_V(y_l) - (\epsilon_l^A)^2 I_A(y_l)\right), \tag{4.23}$$

where $y_l = m_X^2/m_l^2$, and $I_V(y_l)$ and $I_A(y_l)$ are given by

$$I_V(y_l) = \int_0^1 dx \frac{x^2(1-x)}{x^2 + (1-x)y_l}, \tag{4.24a}$$

$$I_A(y_l) = \frac{1}{y_l}\int_0^1 dx \frac{2x^3 + (x-x^2)(4-x)y_l}{x^2 + (1-x)y_l}. \tag{4.24b}$$

It should be noticed that the axial coupling contribution to δa_l is always negative while the vector contribution is positive. The integration of eqs. (4.24) can be done numerically for electron and muon as

$$I_V(y_e) = 6.894 \times 10^{-7}, \quad I_A(y_e) = 3.484 \times 10^{-6}, \tag{4.25a}$$

$$I_V(y_\mu) = 7.881 \times 10^{-4}, \quad I_A(y_\mu) = 9.419 \times 10^{-2}, \tag{4.25b}$$

where we used $m_e = 0.5110\,\text{MeV}$ and $m_\mu = 105.7\,\text{MeV}$, respectively.

The muon anomalous magnetic moment has exhibited a long-standing discrepancy between experimental results [69, 70] and theoretical predictions [71–74]. From [70], the discrepancy is given by

$$\Delta a_\mu = a_\mu^{\text{exp}} - a_\mu^{\text{SM}} = (2.61 \pm 0.79) \times 10^{-9}, \tag{4.26}$$

JHEP04(2021)025

where $a_\mu^{\rm exp}$ and $a_\mu^{\rm SM}$ represent the anomalous magnetic moment by the measurements and SM predictions, respectively. From eqs. (4.25b), one finds that δa_μ can be positive when $|\epsilon_e^V| \gtrsim 10|\epsilon_e^A|$. However, such parameter region is excluded by the constraint from $\pi^0 \to \gamma X$, because the lower bound on ϵ_e^A set by the signal requirement, (4.14), results in too large ϵ_e^V in this situation. Then, the dominant part in δa_μ is the axial coupling term and that negative contribution to δa_μ further worsens the discrepancy. Thus a special care to implement the constraint of Δa_μ is required. Following the discussion in [30], we impose a constraint that the contribution from the X boson should be less than 2σ uncertainty of eq. (4.26),

$$|\delta a_\mu| \lesssim 1.58 \times 10^{-9}. \tag{4.27}$$

This above constraint is scaled by the parameter as

$$|\delta a_\mu| = \frac{e^2}{64\pi^2}(1-Q)^2 I_A(y_\mu)\epsilon_R^2, \tag{4.28}$$

thus it is determined mostly by ϵ_R.

The anomalous magnetic moment of electron, $a_e = (g-2)_e/2$, also has been measured accurately [75, 76], and predicted precisely within the SM [77–80]. Although recent results claimed that a_e also exhibits 2.5σ discrepancy between the measurement and SM predictions, we impose a rather conservative constraint [81] employed in [30],

$$-26 \times 10^{-13} \lesssim \delta a_e \lesssim 8 \times 10^{-13}. \tag{4.29}$$

This constraint is weaker than that from δa_μ due to the smaller value of I_V and I_A.

4.2.4 Effective weak charge

The axial-vector coupling of electron can be restricted by atomic parity violation in Cesium (Cs) [82, 83]. The constraint is given by the measurement of the effective weak charge Q_W of the Cs atom [84]. For the X boson with 17 MeV mass, one obtains the following constraint

$$\Delta Q_W = -\frac{2\sqrt{2}e^2}{G_F}\epsilon_e^A\left[(2Z+N)\epsilon_u^V + (Z+2N)\epsilon_d^V\right]\left(\frac{0.8}{(17.0\text{ MeV})^2}\right) \leq 0.71, \tag{4.30}$$

where $Z = 58$ and $N = 78$ are the number of proton and neutrino in Cs nucleus, respectively.

For $|Q| \ll 1$, ΔQ_W is given by

$$\Delta Q_W \simeq -\frac{2\sqrt{2}e^2}{G_F}\frac{\epsilon_R}{16}\left[(Z+N)\epsilon_R + 4Z\cos\theta_W\epsilon\right]\left(\frac{0.8}{(17.0\text{ MeV})^2}\right) \leq 0.71. \tag{4.31}$$

4.2.5 electron beam dump experiments

Another constraint is obtained by searches for gauge boson at electron beam dump experiments, such as SLAC E141 [85, 86], Orsay [87] and NA64 [88], via bremsstrahlung from electron and nuclei scatterings. The null results of these searches are interpreted as either (1) the gauge boson can not be produced due to very small coupling, or (2) the gauge boson

JHEP04(2021)025

decays rapidly in the dump. For the X boson to satisfy the Atomki signal requirement, the latter one restricts the electron couplings. From the latest result of NA64 [88, 89], one obtain the constraint,

$$\sqrt{(\epsilon_e^V)^2 + (\epsilon_e^A)^2} \geq 6.8 \times 10^{-4} \sqrt{\mathrm{Br}(X \to e^+e^-)}. \tag{4.32}$$

Using the approximate expression of ϵ_e^V and ϵ_e^A, the constraint is given by

$$(\epsilon_R + 4\cos\theta_W \epsilon)^2 + \epsilon_R^2 \geq 7.4 \times 10^{-6}. \tag{4.33}$$

4.2.6 Electron-positron collider experiments

The coupling to electron is also constrained by e^+-e^- collider experiment such as KLOE-2 [90] and BaBar [91] experiments. The most stringent limit on the X boson has been set by KLOE-2, searching for $e^+e^- \to \gamma X$ followed by $X \to e^+e^-$,

$$\sqrt{(\epsilon_e^V)^2 + (\epsilon_e^A)^2} \leq \frac{2 \times 10^{-3}}{\sqrt{\mathrm{Br}(X \to e^+e^-)}}. \tag{4.34}$$

This constraint is weaker than that of electron beam dump experiment.

4.2.7 Parity violating Möller scattering

Vector and axial-vector interactions of the X boson to electrons induce an extra parity violation in Möller scattering. The cross section was measured at the SLAC E158 experiment [92]. The constraint for the X boson with the mass of 17 MeV is given as

$$|\epsilon_e^V \epsilon_e^A| \leq 1 \times 10^{-8}/e^2. \tag{4.35}$$

4.2.8 Vacuum expectation value of S

For consistency, eq. (2.27) must be positive. Since $m_Z^2 \gg m_X^2$, the requirement turns out to be

$$m_X^2(m_Z^2 + r^2(\delta_1^2 + \delta_2^2)) - r^2 m_Z^2 \delta_2^2 - m_X^4 > 0. \tag{4.36}$$

This constraint is also approximated as

$$29 + 6.7\epsilon^2 + 3.0 \times 10^8 q_2 \epsilon_R^2 > 0, \tag{4.37}$$

where we set $Q = 0$ and $q_1 = 1/2$. Thus, the constraint excludes the parameter space when q_2 is negative. Assuming that ϵ is the same order of ϵ_R, the exclusion region for $q_2 < 0$ is given by

$$|\epsilon_R| > \frac{3.1 \times 10^{-4}}{\sqrt{|q_2|}}. \tag{4.38}$$

5 Numerical results

In this section, we show our numerical results of the signal requirement and experimental constraints listed in the previous section. As we explained in section III, the coupling constant of left-handed neutrino in Model 2 and 4 is so large for any value of β that the constraint from neutrino-electron scattering can not be evaded. We have analyzed the signal requirement and the constraints, and found no allowed region in these two models. Therefore, we show our numerical results on Model 1 and 3.

JHEP04(2021)025

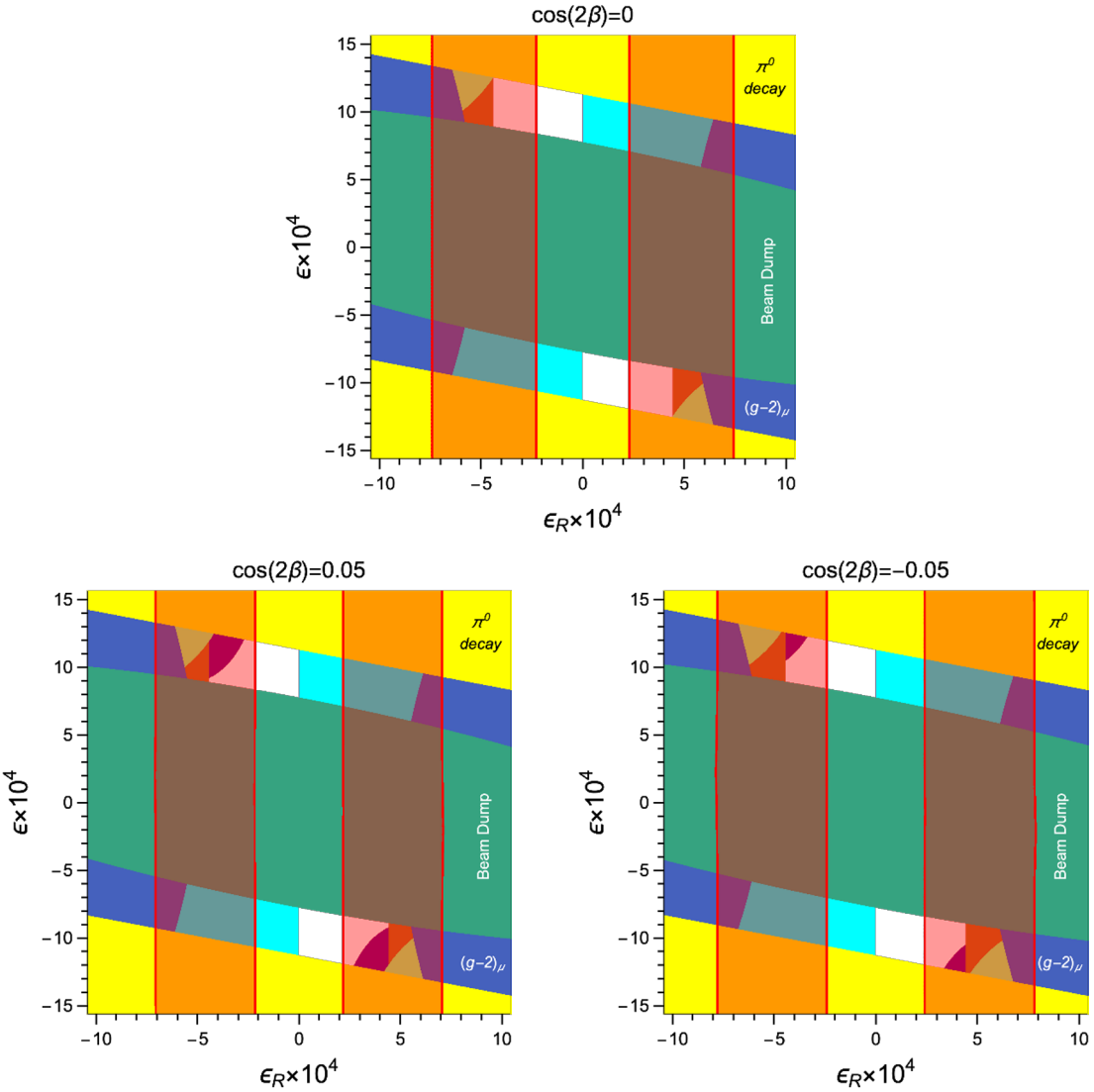

Figure 3. Allowed parameter region and signal in Model 1. The red band is the signal region for the Atomki results. White region is allowed by experiments, while other colored regions are excluded by the constraints from rare π^0 decay (yellow), ν-e scattering (purple), $(g-2)_\mu$ (dark blue), effective weak charge (light blue), electron beam dump (green), and VEV of S (brown).

5.1 Model 1

Figure 3 shows the signal region eq. (4.3) and exclusion regions for Model 1 in ϵ_R-ϵ plane. In this model, the factor Q, which determines the constraints from neutrino-electron scattering and signal, is given by,

$$Q = -\cos 2\beta, \tag{5.1}$$

and hence Q vanishes for $\cos 2\beta = 0$. We took $\cos 2\beta$ to 0 and also 0.05 for comparison as shown in the top of each panels. The mass of X is fixed to be 17.01 MeV for the constraints because the constraints are less sensitive to m_X, while it is taken to be 17.6 and 16.7 MeV

JHEP04(2021)025

for the signals, respectively. The red transparent band represents the signal region with $B_X = 4\times10^{-7}$ (inside) and 7×10^{-6}(outside), respectively. Color filled regions are exclusion region by the experimental constraints from $\pi^0 \to \gamma X$ (yellow), ν-e scattering (purple), muon $g-2$ (dark blue), effective weak charge (light blue), electron beam dump experiment (green) and also by the theoretical constraints from the positive VEV squared of the scalar field S (brown).

We first explain the general behavior of the signal requirement and constraints. In each panel, one can see that the signal requirement is almost determined only by ϵ_R, which is well approximated by eq. (4.14). For $Q = \pm 0.1$, the signal requirement shows slight dependence on ϵ in small $|\epsilon|$ region. In such region, the decay branching ratio of $X \to \nu\nu$ is not negligible, and therefore larger ϵ_R is needed to satisfy the signal by enhancing the decay of $X \to e^+e^-$.

About the constraints, one can also see that the $\pi^0 \to \gamma X$ constraint excludes the region in large $|\epsilon|$ while the constraints from $(g-2)_\mu$ and VEV of S exclude the region in large $|\epsilon_R|$. The central region is excluded by the constraint from electron beam dump experiment. The constraint from effective weak charge excludes the region of $\epsilon\epsilon_R > 0$. The qualitative behavior of these exclusion regions can be understood by the approximated expressions of the constraints, eqs. (4.18), (4.28) and (4.33), (4.38). The last one is the constraints from neutrino-electron scattering, which is well approximated by eq. (4.22) with $\cos 2\beta$ chosen here. It is seen that the constraint excludes large region of the parameter space in $\epsilon\epsilon_R < 0$ for $|\cos 2\beta| = 0.1$, while it disappears for $\cos 2\beta = 0$. This is because $\epsilon_{\rm NC}$ is not suppressed in the former cases. For $\cos 2\beta = 0$ ($Q = 0$), we found wider parameter region consistent with the Atomki signal and all of the constraints. The coupling constants for this region is $2.2 \lesssim |\epsilon_R| \times 10^4 \lesssim 4.4$, $8.4 \lesssim |\epsilon| \times 10^4 \lesssim 12.4$. For $\cos 2\beta = -0.05$, the consistent region in the parameter space is found in $2.4 \lesssim |\epsilon_R| \times 10^4 \lesssim 4.4$ and $8.5 \lesssim |\epsilon| \times 10^4 \lesssim 12.2$, and for $\cos 2\beta = 0.05$, $2.1 \lesssim |\epsilon_R| \times 10^4 \lesssim 4.4$ and $8.4 \lesssim |\epsilon| \times 10^4 \lesssim 12.0$, respectively. For $|\cos 2\beta| \gtrsim 0.1$, there are no consistent region found in our analysis.

5.2 Model 3

Figure 4 is the same plot for model 3 as figure 3. In this model, Q is given by

$$Q = -1 - 2\cos 2\beta, \tag{5.2}$$

and hence we took $\cos 2\beta = -0.5$. The general behavior of the signal requirement and constraints is almost the same as in Model 1. We found a narrow consistent region in the parameter space for $\cos 2\beta = -0.5$. The coupling constant for this region is $2.3 \leq |\epsilon_R| \times 10^4 \leq 2.5$ and $8.5 \leq |\epsilon| \times 10^4 \leq 11.9$. In this model, the constraint from the VEV of S excludes most of the signal region, even if the neutrino-electron scattering constraint is avoided by taking $Q = 0$. From eq. (4.38), the exclusion region from this constraint is obtained as

$$|\epsilon_R| > 2.5 \times 10^{-4}, \tag{5.3}$$

while that in Model 1 is

$$|\epsilon_R| > 4.4 \times 10^{-4}, \tag{5.4}$$

which is in good agreement with our numerical results.

JHEP04(2021)025

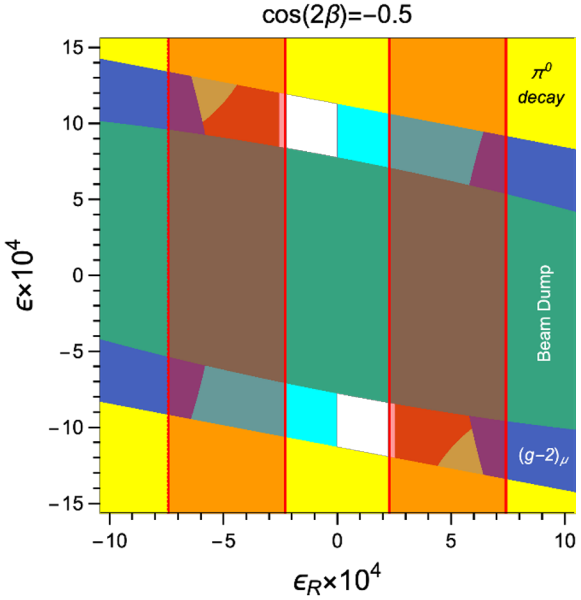

Figure 4. The same figure as figure 3 in Model 3.

6 Conclusion

We have discussed the Atomki anomaly in the gauged $U(1)_R$ symmetric model. As a minimal model to solve the anomaly, three right-handed neutrinos are introduced for the cancellation of gauge anomalies. Two SU(2) doublet and one SM singlet Higgs scalar particles are also introduced to evade the stringent constraints from neutrino-electron scattering and relativistic degree at the early Universe. Then, the new gauge boson is identified with the $X17$ boson. The Atomki signal requirement and other experimental constraints have been studied analytically and numerically in this model.

We first classified the models depending on the $U(1)_R$ charges of two doublet Higgs fields, by requiring all of CP-odd as well as the CP-even scalars to be massive. We found that the possible choices of the gauge charges are limited to four cases $q_2 = -1/2,\ \pm 3/2,\ +5/2$. Two of them leads to large neutrino coupling to electron, and hence such cases are excluded by the constraint from neutrino-electron scattering. Then, for other models with $q_2 = -1/2$ and $-3/2$, called Model 1 and 3 respectively, we found that consistent regions with the signal and constraints exist. In such regions, the constraint from neutrino-electron scattering is suppressed due to the cancellation of the gauge charges between two Higgs doublets. In Model 1, the consistent region can be found for $|\cos 2\beta| < 0.05$ and in Model 3, it is found for $\cos 2\beta = -0.5$. Other values of $\cos\beta$ and also other models have been excluded by experimental and theoretical constraints.

Comment. While we were finishing this work, ref. [35] appeared, in which the axial-vector hypothesis was examined. The authors concluded that ^{8}Be and ^{4}He anomalies could be explained by significant uncertainty in nuclear matrix elements.

JHEP04(2021)025

Acknowledgments

This work is supported, in part, by JSPS KAKENHI Grant Nos. 19K03860 and 19K03865, and MEXT KAKENHI Grant No. 19H05091 (O.S.), and JSPS KAKENHI Grant Nos. 18K03651, 18H01210 and MEXT KAKENHI Grant No. 18H05543 (T.S.).

JHEP04(2021)025

References

[1] A.J. Krasznahorkay et al., *Observation of anomalous internal pair creation in ^{8}Be: a possible indication of a light, neutral boson*, *Phys. Rev. Lett.* **116** (2016) 042501 [arXiv:1504.01527] [INSPIRE].

[2] A.J. Krasznahorkay et al., *New experimental results for the 17 MeV particle created in ^{8}Be*, *EPJ Web Conf.* **137** (2017) 08010 [INSPIRE].

[3] A.J. Krasznahorkay et al., *On the creation of the 17 MeV X boson in the 17.6 MeV M1 transition of ^{8}Be*, *EPJ Web Conf.* **142** (2017) 01019 [INSPIRE].

[4] A.J. Krasznahorkay et al., *New results on the ^{8}Be anomaly*, PoS(BORMIO2017)036 [INSPIRE].

[5] A.J. Krasznahorkay et al., *New results on the ^{8}Be anomaly*, *J. Phys. Conf. Ser.* **1056** (2018) 012028 [INSPIRE].

[6] A.J. Krasznahorkay et al., *New evidence supporting the existence of the hypothetic X17 particle*, arXiv:1910.10459 [INSPIRE].

[7] D.S. Firak et al., *Confirmation of the existence of the X17 particle*, *EPJ Web Conf.* **232** (2020) 04005 [INSPIRE].

[8] X. Zhang and G.A. Miller, *Can nuclear physics explain the anomaly observed in the internal pair production in the Beryllium-8 nucleus?*, *Phys. Lett. B* **773** (2017) 159 [arXiv:1703.04588] [INSPIRE].

[9] J.L. Feng et al., *Protophobic fifth-force interpretation of the observed anomaly in ^{8}Be nuclear transitions*, *Phys. Rev. Lett.* **117** (2016) 071803 [arXiv:1604.07411] [INSPIRE].

[10] J.L. Feng et al., *Particle physics models for the 17 MeV anomaly in beryllium nuclear decays*, *Phys. Rev. D* **95** (2017) 035017 [arXiv:1608.03591] [INSPIRE].

[11] P.-H. Gu and X.-G. He, *Realistic model for a fifth force explaining anomaly in $^8Be^* \to {}^8Be\, e^+e^-$ decay*, *Nucl. Phys. B* **919** (2017) 209 [arXiv:1606.05171] [INSPIRE].

[12] M.J. Neves, E.M.C. Abreu and J.A. Helayël-Neto, *The protophobic X-boson coupled to quantum electrodynamics*, *Acta Phys. Polon. B* **51** (2020) 909 [arXiv:1704.02491] [INSPIRE].

[13] B. Puliçe, *A family-nonuniversal U(1)′ model for excited beryllium decays*, arXiv:1911.10482 [INSPIRE].

[14] T. Kitahara and Y. Yamamoto, *Protophobic light vector boson as a mediator to the dark sector*, *Phys. Rev. D* **95** (2017) 015008 [arXiv:1609.01605] [INSPIRE].

[15] L.-B. Jia, *Explanation of the 511 keV line: cascade annihilating dark matter with the ^{8}Be anomaly*, *Eur. Phys. J. C* **78** (2018) 112 [arXiv:1710.03906] [INSPIRE].

[16] L.-B. Jia, X.-J. Deng and C.-F. Liu, *Could the 21-cm absorption be explained by the dark matter suggested by* ^{8} *Be transitions?*, *Eur. Phys. J. C* **78** (2018) 956 [arXiv:1809.00177] [INSPIRE].

[17] O. Seto and T. Shimomura, *Atomki anomaly and dark matter in a radiative seesaw model with gauged B-L symmetry*, *Phys. Rev. D* **95** (2017) 095032 [arXiv:1610.08112] [INSPIRE].

[18] J. Bordes, H.-M. Chan and S.T. Tsou, *Accommodating three low-scale anomalies ($g-2$, Lamb shift, and Atomki) in the framed standard model*, *Int. J. Mod. Phys. A* **34** (2019) 1950140 [arXiv:1906.09229] [INSPIRE].

[19] D.V. Kirpichnikov, V.E. Lyubovitskij and A.S. Zhevlakov, *Implication of hidden sub-GeV bosons for the* $(g-2)_\mu$, ^{8}*Be-*^{4}*He anomaly, proton charge radius, EDM of fermions, and dark axion portal*, *Phys. Rev. D* **102** (2020) 095024 [arXiv:2002.07496] [INSPIRE].

[20] C. Hati, J. Kriewald, J. Orloff and A.M. Teixeira, *Anomalies in* ^{8}*Be nuclear transitions and* $(g-2)_{e,\mu}$*: towards a minimal combined explanation*, *JHEP* **07** (2020) 235 [arXiv:2005.00028] [INSPIRE].

[21] M.J. Neves, L. Labre, L.S. Miranda and E.M.C. Abreu, *Classical electrodynamics and gauge symmetry of the X-boson*, *Int. J. Mod. Phys. A* **33** (2018) 1850148 [arXiv:1802.10449] [INSPIRE].

[22] C.H. Nam, 17 *MeV Atomki anomaly from short-distance structure of spacetime*, *Eur. Phys. J. C* **80** (2020) 231 [arXiv:1907.09819] [INSPIRE].

[23] C.-Y. Wong, *Open string QED meson description of the X17 particle and dark matter*, *JHEP* **08** (2020) 165 [arXiv:2001.04864] [INSPIRE].

[24] E.M. Tursunov, *Evidence of quantum phase transition in carbon-12 in a* 3α *model and the problem of hypothetical X17 boson*, arXiv:2001.08995 [INSPIRE].

[25] H.-X. Chen, *Is the X17 composed of four bare quarks?*, arXiv:2006.01018 [INSPIRE].

[26] I. Alikhanov and E.A. Paschos, *Searching for new light gauge bosons at* e^+e^- *colliders*, *Phys. Rev. D* **97** (2018) 115004 [arXiv:1710.10131] [INSPIRE].

[27] U.D. Jentschura and I. Nándori, *Atomic physics constraints on the X boson*, *Phys. Rev. A* **97** (2018) 042502 [arXiv:1804.03096] [INSPIRE].

[28] B. Koch, *X17: A new force, or evidence for a hard* $\gamma+\gamma$ *process?*, *Nucl. Phys. A* **1008** (2021) 122143 [arXiv:2003.05722] [INSPIRE].

[29] U.D. Jentschura, *Fifth force and hyperfine splitting in bound systems*, *Phys. Rev. A* **101** (2020) 062503 [arXiv:2003.07207] [INSPIRE].

[30] J. Kozaczuk, D.E. Morrissey and S.R. Stroberg, *Light axial vector bosons, nuclear transitions, and the* ^{8}*Be anomaly*, *Phys. Rev. D* **95** (2017) 115024 [arXiv:1612.01525] [INSPIRE].

[31] L. Delle Rose, S. Khalil and S. Moretti, *Explanation of the* 17 *MeV Atomki anomaly in a* U(1)$'$*-extended two Higgs doublet model*, *Phys. Rev. D* **96** (2017) 115024 [arXiv:1704.03436] [INSPIRE].

[32] L. Delle Rose, S. Khalil, S.J.D. King, S. Moretti and A.M. Thabt, *Atomki anomaly in family-dependent* U(1)$'$ *extension of the standard model*, *Phys. Rev. D* **99** (2019) 055022 [arXiv:1811.07953] [INSPIRE].

[33] L. Delle Rose, S. Khalil, S.J.D. King and S. Moretti, *New physics suggested by Atomki anomaly*, *Front. in Phys.* **7** (2019) 73 [arXiv:1812.05497] [INSPIRE].

[34] U. Ellwanger and S. Moretti, *Possible explanation of the electron positron anomaly at* 17 *MeV in* ^{8}*Be transitions through a light pseudoscalar*, *JHEP* **11** (2016) 039 [arXiv:1609.01669] [INSPIRE].

JHEP04(2021)025

[35] J.L. Feng, T.M.P. Tait and C.B. Verhaaren, *Dynamical evidence for a fifth force explanation of the ATOMKI nuclear anomalies*, *Phys. Rev. D* **102** (2020) 036016 [arXiv:2006.01151] [INSPIRE].

[36] S. Jung, H. Murayama, A. Pierce and J.D. Wells, *Top quark forward-backward asymmetry from new t-channel physics*, *Phys. Rev. D* **81** (2010) 015004 [arXiv:0907.4112] [INSPIRE].

[37] P. Ko, Y. Omura and C. Yu, *A resolution of the flavor problem of two Higgs doublet models with an extra* $\mathrm{U}(1)_H$ *symmetry for Higgs flavor*, *Phys. Lett. B* **717** (2012) 202 [arXiv:1204.4588] [INSPIRE].

[38] P. Ko, Y. Omura and C. Yu, *Higgs phenomenology in Type-I 2HDM with* $\mathrm{U}(1)_H$ *Higgs gauge symmetry*, *JHEP* **01** (2014) 016 [arXiv:1309.7156] [INSPIRE].

[39] T. Nomura and H. Okada, *Loop suppressed light fermion masses with* $\mathrm{U}(1)_R$ *gauge symmetry*, *Phys. Rev. D* **96** (2017) 015016 [arXiv:1704.03382] [INSPIRE].

[40] T. Nomura and H. Okada, *Minimal realization of right-handed gauge symmetry*, *Phys. Rev. D* **97** (2018) 015015 [arXiv:1707.00929] [INSPIRE].

[41] T. Nomura and H. Okada, *An inverse seesaw model with* $\mathrm{U}(1)_R$ *gauge symmetry*, *LHEP* **1** (2018) 10 [arXiv:1806.01714] [INSPIRE].

[42] W. Chao, *Phenomenology of the gauge symmetry for right-handed fermions*, *Eur. Phys. J. C* **78** (2018) 103 [arXiv:1707.07858] [INSPIRE].

[43] S. Jana, V.P.K. and S. Saad, *Minimal Dirac neutrino mass models from* $\mathrm{U}(1)_R$ *gauge symmetry and left-right asymmetry at colliders*, *Eur. Phys. J. C* **79** (2019) 916 [arXiv:1904.07407] [INSPIRE].

[44] J. Heeck, *Unbroken B-L symmetry*, *Phys. Lett. B* **739** (2014) 256 [arXiv:1408.6845] [INSPIRE].

[45] J.E. Kim and G. Carosi, *Axions and the strong CP problem*, *Rev. Mod. Phys.* **82** (2010) 557 [*Erratum ibid.* **91** (2019) 049902] [arXiv:0807.3125] [INSPIRE].

[46] M. Kawasaki and K. Nakayama, *Axions: theory and cosmological role*, *Ann. Rev. Nucl. Part. Sci.* **63** (2013) 69 [arXiv:1301.1123] [INSPIRE].

[47] ATLAS collaboration, *Search for Higgs boson decays to beyond-the-Standard-Model light bosons in four-lepton events with the ATLAS detector at* $\sqrt{s} = 13$ *TeV*, *JHEP* **06** (2018) 166 [arXiv:1802.03388] [INSPIRE].

[48] ATLAS collaboration, *Combination of searches for invisible Higgs boson decays with the ATLAS experiment*, *Phys. Rev. Lett.* **122** (2019) 231801 [arXiv:1904.05105] [INSPIRE].

[49] ATLAS collaboration, *Combined measurements of Higgs boson production and decay using up to* 80 fb^{-1} *of proton-proton collision data at* $\sqrt{s} = 13$ *TeV collected with the ATLAS experiment*, *Phys. Rev. D* **101** (2020) 012002 [arXiv:1909.02845] [INSPIRE].

[50] Y. Tsai, L.-T. Wang and Y. Zhao, *Faking ordinary photons by displaced dark photon decays*, *Phys. Rev. D* **95** (2017) 015027 [arXiv:1603.00024] [INSPIRE].

[51] C.-Y. Chen, M. Lefebvre, M. Pospelov and Y.-M. Zhong, *Diphoton excess through dark mediators*, *JHEP* **07** (2016) 063 [arXiv:1603.01256] [INSPIRE].

[52] ATLAS collaboration, *Search for new phenomena in high-mass diphoton final states using* 37 fb^{-1} *of proton-proton collisions collected at* $\sqrt{s} = 13$ *TeV with the ATLAS detector*, *Phys. Lett. B* **775** (2017) 105 [arXiv:1707.04147] [INSPIRE].

[53] CMS collaboration, *Search for physics beyond the standard model in high-mass diphoton events from proton-proton collisions at* $\sqrt{s} = 13$ *TeV*, *Phys. Rev. D* **98** (2018) 092001 [arXiv:1809.00327] [INSPIRE].

JHEP04(2021)025

[54] ATLAS collaboration, *Search for heavy resonances decaying into a pair of Z bosons in the $\ell^+\ell^-\ell'^+\ell'^-$ and $\ell^+\ell^-\nu\bar{\nu}$ final states using 139 fb^{-1} of proton-proton collisions at $\sqrt{s} = 13$ TeV with the ATLAS detector*, arXiv:2009.14791 [INSPIRE].

[55] ATLAS collaboration, *Search for heavy Higgs bosons decaying into two tau leptons with the ATLAS detector using pp collisions at $\sqrt{s} = 13$ TeV*, *Phys. Rev. Lett.* **125** (2020) 051801 [arXiv:2002.12223] [INSPIRE].

[56] ATLAS collaboration, *Search for charged Higgs bosons decaying into top and bottom quarks at $\sqrt{s} = 13$ TeV with the ATLAS detector*, *JHEP* **11** (2018) 085 [arXiv:1808.03599] [INSPIRE].

[57] J. Haller, A. Hoecker, R. Kogler, K. Mönig, T. Peiffer and J. Stelzer, *Update of the global electroweak fit and constraints on two-Higgs-doublet models*, *Eur. Phys. J. C* **78** (2018) 675 [arXiv:1803.01853] [INSPIRE].

[58] N. Chen, T. Han, S. Li, S. Su, W. Su and Y. Wu, *Type-I 2HDM under the Higgs and Electroweak Precision Measurements*, *JHEP* **08** (2020) 131 [arXiv:1912.01431] [INSPIRE].

[59] J.A. Dror, R. Lasenby and M. Pospelov, *New constraints on light vectors coupled to anomalous currents*, *Phys. Rev. Lett.* **119** (2017) 141803 [arXiv:1705.06726] [INSPIRE].

[60] J.A. Dror, R. Lasenby and M. Pospelov, *Dark forces coupled to nonconserved currents*, *Phys. Rev. D* **96** (2017) 075036 [arXiv:1707.01503] [INSPIRE].

[61] Y. Kahn, G. Krnjaic, S. Mishra-Sharma and T.M.P. Tait, *Light weakly coupled axial forces: models, constraints, and projections*, *JHEP* **05** (2017) 002 [arXiv:1609.09072] [INSPIRE].

[62] Particle Data Group collaboration, *Review of particle physics*, *Phys. Rev. D* **98** (2018) 030001 [INSPIRE].

[63] TEXONO collaboration, *Final results of nu-e-bar electron scattering cross-section measurements and constraints on new physics*, *J. Phys. Conf. Ser.* **375** (2012) 042044 [arXiv:1201.4675] [INSPIRE].

[64] F. Bishara, J. Brod, B. Grinstein and J. Zupan, *Chiral effective theory of dark matter direct detection*, *JCAP* **02** (2017) 009 [arXiv:1611.00368] [INSPIRE].

[65] NA48/2 collaboration, *NA48/2 studies of rare decays*, *Nuovo Cim. C* **38** (2016) 132 [arXiv:1508.01307] [INSPIRE].

[66] M. Lindner, F.S. Queiroz, W. Rodejohann and X.-J. Xu, *Neutrino-electron scattering: general constraints on Z' and dark photon models*, *JHEP* **05** (2018) 098 [arXiv:1803.00060] [INSPIRE].

[67] S. Bilmis, I. Turan, T.M. Aliev, M. Deniz, L. Singh and H.T. Wong, *Constraints on dark photon from neutrino-electron scattering experiments*, *Phys. Rev. D* **92** (2015) 033009 [arXiv:1502.07763] [INSPIRE].

[68] P. Fayet, *U-boson production in e^+e^- annihilations, ψ and Υ decays, and light dark matter*, *Phys. Rev. D* **75** (2007) 115017 [hep-ph/0702176] [INSPIRE].

[69] Muon g-2 collaboration, *Final report of the muon E821 anomalous magnetic moment measurement at BNL*, *Phys. Rev. D* **73** (2006) 072003 [hep-ex/0602035] [INSPIRE].

[70] Particle Data Group collaboration, *Review of particle physics*, *Prog. Theor. Exp. Phys.* **2020**1 (2020) 083C01.

[71] M. Davier, A. Hoecker, B. Malaescu and Z. Zhang, *Reevaluation of the hadronic vacuum polarisation contributions to the Standard Model predictions of the muon $g-2$ and $\alpha(m_Z^2)$ using newest hadronic cross-section data*, *Eur. Phys. J. C* **77** (2017) 827 [arXiv:1706.09436] [INSPIRE].

JHEP04(2021)025

[72] A. Keshavarzi, D. Nomura and T. Teubner, *Muon $g-2$ and $\alpha(M_Z^2)$: a new data-based analysis*, *Phys. Rev. D* **97** (2018) 114025 [arXiv:1802.02995] [INSPIRE].

[73] RBC, UKQCD collaboration, *Calculation of the hadronic vacuum polarization contribution to the muon anomalous magnetic moment*, *Phys. Rev. Lett.* **121** (2018) 022003 [arXiv:1801.07224] [INSPIRE].

[74] M. Davier, A. Hoecker, B. Malaescu and Z. Zhang, *A new evaluation of the hadronic vacuum polarisation contributions to the muon anomalous magnetic moment and to $\alpha(m_Z^2)$*, *Eur. Phys. J. C* **80** (2020) 241 [*Erratum ibid.* **80** (2020) 410] [arXiv:1908.00921] [INSPIRE].

[75] D. Hanneke, S. Fogwell and G. Gabrielse, *New measurement of the electron magnetic moment and the fine structure constant*, *Phys. Rev. Lett.* **100** (2008) 120801 [arXiv:0801.1134] [INSPIRE].

[76] D. Hanneke, S.F. Hoogerheide and G. Gabrielse, *Cavity control of a single-electron quantum cyclotron: measuring the electron magnetic moment*, *Phys. Rev. A* **83** (2011) 052122 [arXiv:1009.4831] [INSPIRE].

[77] T. Aoyama, M. Hayakawa, T. Kinoshita and M. Nio, *Tenth-order QED contribution to the electron $g-2$ and an improved value of the fine structure constant*, *Phys. Rev. Lett.* **109** (2012) 111807 [arXiv:1205.5368] [INSPIRE].

[78] T. Aoyama, M. Hayakawa, T. Kinoshita and M. Nio, *Tenth-order electron anomalous magnetic moment — Contribution of diagrams without closed lepton loops*, *Phys. Rev. D* **91** (2015) 033006 [*Erratum ibid.* **96** (2017) 019901] [arXiv:1412.8284] [INSPIRE].

[79] S. Laporta, *High-precision calculation of the 4-loop contribution to the electron $g-2$ in QED*, *Phys. Lett. B* **772** (2017) 232 [arXiv:1704.06996] [INSPIRE].

[80] T. Aoyama, T. Kinoshita and M. Nio, *Revised and improved value of the QED tenth-order electron anomalous magnetic moment*, *Phys. Rev. D* **97** (2018) 036001 [arXiv:1712.06060] [INSPIRE].

[81] G.F. Giudice, P. Paradisi and M. Passera, *Testing new physics with the electron $g-2$*, *JHEP* **11** (2012) 113 [arXiv:1208.6583] [INSPIRE].

[82] C. Bouchiat and P. Fayet, *Constraints on the parity-violating couplings of a new gauge boson*, *Phys. Lett. B* **608** (2005) 87 [hep-ph/0410260] [INSPIRE].

[83] H. Davoudiasl, H.-S. Lee and W.J. Marciano, *'Dark' Z implications for parity violation, rare meson decays, and Higgs physics*, *Phys. Rev. D* **85** (2012) 115019 [arXiv:1203.2947] [INSPIRE].

[84] S.G. Porsev, K. Beloy and A. Derevianko, *Precision determination of electroweak coupling from atomic parity violation and implications for particle physics*, *Phys. Rev. Lett.* **102** (2009) 181601 [arXiv:0902.0335] [INSPIRE].

[85] E.M. Riordan et al., *A search for short lived axions in an electron beam dump experiment*, *Phys. Rev. Lett.* **59** (1987) 755 [INSPIRE].

[86] J.D. Bjorken, R. Essig, P. Schuster and N. Toro, *New fixed-target experiments to search for dark gauge forces*, *Phys. Rev. D* **80** (2009) 075018 [arXiv:0906.0580] [INSPIRE].

[87] M. Davier and H. Nguyen Ngoc, *An unambiguous search for a light Higgs boson*, *Phys. Lett. B* **229** (1989) 150 [INSPIRE].

[88] NA64 collaboration, *Search for a hypothetical* 16.7 *MeV gauge boson and dark photons in the NA64 experiment at CERN*, *Phys. Rev. Lett.* **120** (2018) 231802 [arXiv:1803.07748] [INSPIRE].

JHEP04(2021)025

[89] NA64 collaboration, *Improved limits on a hypothetical X(16.7) boson and a dark photon decaying into e^+e^- pairs*, *Phys. Rev. D* **101** (2020) 071101 [arXiv:1912.11389] [INSPIRE].

[90] A. Anastasi et al., *Limit on the production of a low-mass vector boson in $e^+e^- \to U\gamma$, $U \to e^+e^-$ with the KLOE experiment*, *Phys. Lett. B* **750** (2015) 633 [arXiv:1509.00740] [INSPIRE].

[91] BABAR collaboration, *Search for a dark photon in e^+e^- collisions at BaBar*, *Phys. Rev. Lett.* **113** (2014) 201801 [arXiv:1406.2980] [INSPIRE].

[92] SLAC E158 collaboration, *Precision measurement of the weak mixing angle in Möller scattering*, *Phys. Rev. Lett.* **95** (2005) 081601 [hep-ex/0504049] [INSPIRE].

JHEP04(2021)025